Adsorption and Surface Reactivity on Single-Walled Boron Nitride Nanotubes Containing Stone–Wales Defects

ARTICLE *in* THE JOURNAL OF PHYSICAL CHEMISTRY C · AUGUST 2007

Impact Factor: 4.77 · DOI: 10.1021/jp072443w

4 AUTHORS, INCLUDING:

Wei An
Shanghai University of Engineering Science
47 PUBLICATIONS **1,097** CITATIONS
SEE PROFILE

Xiaojun Wu
University of Science and Technology of China
116 PUBLICATIONS **2,354** CITATIONS
SEE PROFILE

Jinlong Yang
University of Science and Technology of China
524 PUBLICATIONS **11,180** CITATIONS
SEE PROFILE

Adsorption and Surface Reactivity on Single-Walled Boron Nitride Nanotubes Containing Stone−Wales Defects

Wei An,[†] Xiaojun Wu,[†] J. L. Yang,[‡] and X. C. Zeng*[,†]

Department of Chemistry and Nebraska Center for Materials and Nanoscience, University of Nebraska-Lincoln, Lincoln, Nebraska 68588, and Hefei National Laboratory for Physical Science at Microscale and Department of Chemical Physics, University of Science and Technology of China, Hefei, 230026, China

Received: March 28, 2007; In Final Form: July 16, 2007

Adsorption of chemical species H, O, CO, H_2, O_2, H_2O, and NH_3 on the sidewall of zigzag (8,0) and armchair (5, 5) boron nitride nanotubes (BNNTs) is studied using density-functional theory. Particular attention is paid to searching for the most-stable configuration of the adsorbates at a perfect site (PS) and near a Stone−Wales (SW) defect, and the surface reactivity at the PS and near the SW defect. Reactivity near the SW defect is generally higher than that at the PS because of the formation of frustrated B−B and N−N bonds and the local strain caused by pentagonal and heptagonal pairs. O_2 is prone to dissociative chemisorption near SW defects, but is more likely physisorbed at the PS. The adsorption of H_2O and NH_3 on the sidewall of BNNT can be described as molecular chemisorption due to modest interaction between HOMO of H_2O or NH_3 with LUMO of BNNT. Adsorption of NH_3 can affect electronic properties of BNNT through lifting the Fermi level. As such, NH_3 can be viewed as an *n*-type impurity. CO and H_2 can only be physisorbed on the sidewall of BNNT through van der Waals interactions.

1. Introduction

Bulk boron nitride (BN) is a non-oxide ceramic and has been widely used in industrial applications because of its unique physical, chemical, and electronic properties such as high melting point, low density, high thermal conductivity, chemical inertness, and insulating characteristics.[1] In bulk hexagonal boron nitride (*h*-BN), the B−N sp^2-hybrid bonds are arranged uniformly. In contrast, substantial buckling of B−N sp^2 bonds occurs in zigzag BN nanotubes (BNNTs), which gives rise to a dipole shell between the inner B-atom cylinder and the outer N-atom cylinder as a result of charge transfer from boron to nitrogen.[2−4] Hence, BNNTs can exhibit novel surface effects that cannot be seen in their bulk counterparts. Alternatively, BNNTs also inherit some intrinsic properties of bulk BN, such as insulating characteristics with a large band gap of ca. 5.5 eV (compared with 5.8 eV for bulk *h*-BN and 6.3 eV for *c*-BN)[4,5] as well as chemical oxidation inertness.[6]

The single-walled and multiwalled BNNTs exhibit nearly constant band gaps independent of the chirality of BNNTs and the tube diameter.[4] These properties of BNNTs are in stark contrast to those of carbon nanotubes (CNTs) whose electronic properties are dependent on the chiral index (*n*, *m*). It is known that a single-walled CNT is metallic if $n - m = 3k$ (where *k* is an integer) or semiconducting if otherwise.[7] Moreover, it is difficult to control the chirality of CNTs, at least with the synthesis techniques to date. Thus, BNNTs have certain practical advantage over CNTs as far as the control of electronic properties is concerned. Indeed, their unique electronic properties associated with thermal and chemical stability and mechanical toughness render BNNTs a promising medium for applications in field emission, protective tubular shields, nanotransistors, and gas sensors in extreme environments.

Pristine BNNTs were first fabricated using the arc discharge method.[8] Since then, many studies have been published on microscopic growth mechanisms, structural characterization, and on the mechanical, optical, and electronic properties of BNNTs (ref 9 and references therein). Because of their large surface-to-mass ratio and their potential applications in miniaturized chemical sensors, the adsorption properties of CNTs and BNNTs have also received considerable attentions. Thus far, most studies of adsorption have been focused on CNTs, and to a lesser extent, on BNNTs.[10−38] For example, adsorption of small molecules such as H_2,[10−14] O_2,[13−18] N_2,[14,17−19] NH_3,[14,15,20−23] NO_2,[14,15,21−24] H_2O,[14,15,17,25] alkanes (C_1-nC_5),[13,14,26,29] O_3,[27a] CO,[15,17] CO_2,[13,14,17,28] Ne,[29] Ar,[13,14,30] and Xe,[29] HF,[17] CF_4[32], NO_2,[31] and some relevant addends such as O, SiH_2, NH, and CH_2[27a,c,53a] on CNTs has been reported. Adsorption of hydrogen on CNTs and BNNTs has drawn intense research interest because both types of nanotubes have been considered as potential H_2-storage media. For BNNTs, a number of theoretical studies of adsorption of H atoms (or H_2 molecules) have been published in the literature.[33−40] Experimental efforts have also been made to chemically functionalize BNNTs with different chemical groups to enhance the solubility of BNNTs in solvent or to tailor their electronic properties.[41,42] To our knowledge, no theoretical studies have been reported on the adsorption of small molecules other than H, H_2, F, and F_2 (refs 27b, 27c, 37, and 40) on BNNTs.

Synthesized BNNTs are mostly nonhelical-type with the [10$\bar{1}$0] direction parallel to the tube axis, known as a "zigzag" arrangement.[2,43−46] However, the formation of armchair BNNTs cannot be absolutely ruled out as shown by previous first-principles molecular dynamics simulations.[2] In the process of preparations or modifications, various types of defects on BNNTs can be formed, such as B or N vacancies, C and transition-metal doping, or topological defects.[9] The Stone−Wales (SW) defect[47] is an arrangement of pentagon/heptagon pairs in adjacent positions (with notation 5-7-7-5). The SW

* Corresponding author. E-mail: xczeng@phase2.unl.edu.
[†] University of Nebraska-Lincoln.
[‡] University of Science and Technology of China.

10.1021/jp072443w CCC: $37.00
Published on Web 08/30/2007

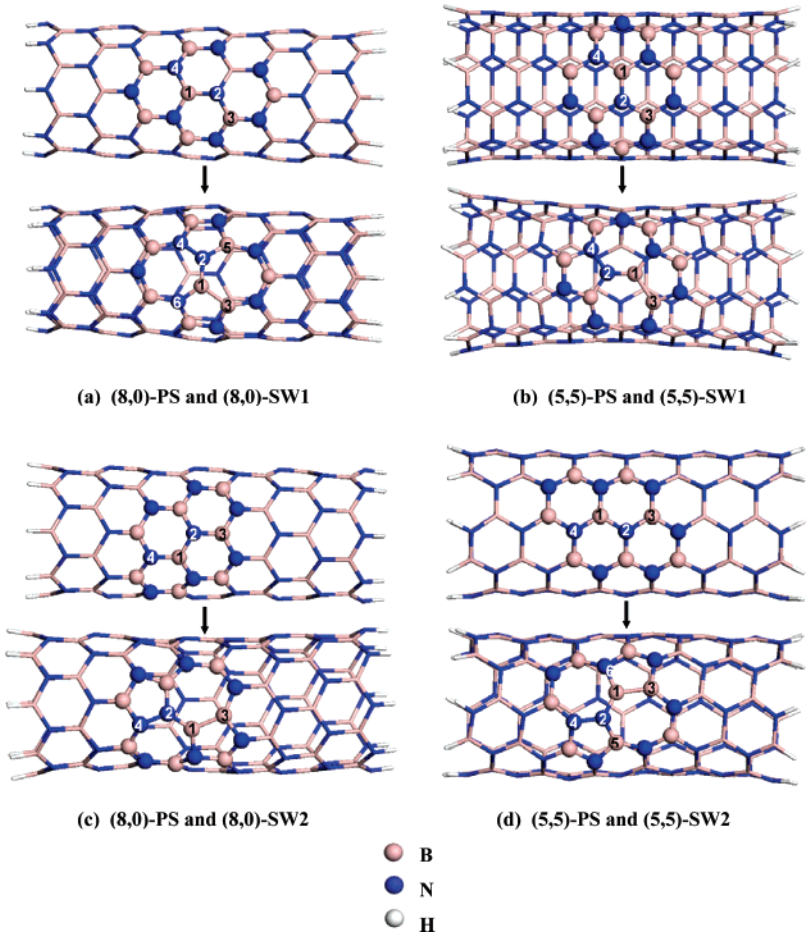

Figure 1. Optimized structures of single-walled zigzag (8,0) and armchair (5, 5) BNNT models. The Stone-Walls (SW) defect site is generated by rotating the B1−N2 bond by 90° with four associated hexagons fusing into two pentagon/heptagon pairs (5-7-7-5). (a and b) Straight SW defect (SW1); (c and d) slanted SW defect (SW2).

defect can be generated in either nonequilibrium microscopic growth of BNNTs or via certain external perturbations,[48−51] even though the energy cost is higher because of the formation of energetically unfavorable N−N and B−B bonds.[2,48−51] It has been suggested that the SW defects may play a key role in the structural reconstruction of graphitic nanostructures.[52]

Chemical reactivities near the SW defect on the sidewall of CNTs (refs 27a, 53, and 54) and BNNTs (refs 35, and 37c,) have been studied recently. An earlier theoretical study of the sidewall reactivity based on a seven-layer armchair (5, 5) CNT model in reacting with O, CH_2, and O_3 species suggested that the SW defect on CNT was more chemically stable than the perfect site (PS).[27a] A later theoretical study reversed the conclusion by using a 10-layer armchair (5, 5) CNT model with periodic boundary conditions (PBCs).[53] Unlike CNTs whose nonpolar C−C bonds form a uniform and smooth sidewall structure, BNNTs contain polar B−N bonds with ionic character, which can induce an extra dipole moment within the tube structure and result in a buckled tubular structure.[2−4] This major structural difference between CNTs and BNNTs motivated us to perform a study of adsorption properties of BNNTs, similar to those for CNTs by other researchers.[27a,53] In this paper, we present a theoretical study of adsorption and the sidewall reactivity of both zigzag (8,0) and armchair (5,5) BNNTs with a number of adsorbates relevant to chemical gas sensors. In particular, we focus on the difference in reactivity at a perfect site and near a SW defect on the sidewall of BNNTs.

2. Theoretical and Computational Details

All-electron density-functional theory (DFT) calculations were carried out using the Gaussian 03, Revision C.02 package.[55] A hybrid exchange-correlation functional PBE1PBE (ref 56) within generalized-gradient approximation (GGA) together with the 6-31G(d) basis sets were employed to optimize the geometric structures of BNNTs, with and without the adsorbates, and to compute the adsorption energies for the adsorbates at the PS or near a SW defect.

Two models of finite-sized BNNT, a 16-layer zigzag (8,0) $B_{64}N_{64}H_{16}$, and a 13-layer armchair (5,5) $B_{65}N_{65}H_{20}$, were considered to represent the defect-free and defect-containing BNNTs, where the two ends of the finite-sized tubes are saturated with H atoms. Our test calculations have shown that a seven-layer armchair model ($B_{35}N_{35}H_{20}$) is too small to give a quantitative description of the binding interaction between an adsorbate and the BNNT. This is in stark contrast to the CNT case for which a seven-layer armchair model has been shown to be sufficiently large.[27a] A perfect site and a Stone-Walls defect on the two model BNNTs are denoted by (8,0)-PS, (5,5)-PS, and (8,0)-SW, (5,5)-SW, respectively (Figure 1). Atomic H and O, and molecular CO, H_2, O_2, H_2O, and NH_3 were considered as probe adsorbates to examine the sidewall reactivity of BNNTs.

The gas molecules and pristine BNNTs were first optimized separately using the PBE1PBE/6-31G(d) level of theory. Next, the combined adsorbate/BNNT systems were fully optimized without any symmetry constraint. A previous study has shown

TABLE 1: Calculated Bond Lengths of Adsorbates and Typical Bond Lengths in (8,0)-PS and -SW1 BNNTs and (5,5)-PS and -SW2 BNNTs as Displayed in Figure 1a and d

	bond length (Å)				bond length (Å)	
	(8,0)-PS	(8,0)-SW1	(5,5)-PS	(5,5)-SW2	adsorbates	bond length
B1−N2	1.445	1.420	1.448	1.411	O_2	1.203
B1−N4	1.450		1.448		H_2O	0.961
B3−N2	1.450		1.448		NH_3	1.015
B−H	1.195	1.195	1.202	1.202	CO	1.135
N−H	1.012	1.012	1.010	1.011	H_2	0.744
B1−B3		1.709		1.694		
N2−N4		1.443		1.429		
B1−N6		1.461		1.450		
N2−B5		1.490		1.471		

that different initial configurations may affect the final results significantly, leading to different conclusions.[27d] Thus, several initial configurations of adsorbates were attempted. For example, we examined different orientations of adsorbates at several locations of the sidewall such as on top of B−B, N−N, B−N bonds, on top of B and N atoms, and on top of hollow sites of B_3N_3 hexagon, B_2N_3 and B_3N_2 pentagons, and B_3N_4 and B_4N_3 heptagons (Figure 1), where the initial distance between adsorbates and the sidewall is set at about 1.2 Å. On the basis of these initial configurations, the binding nature of adsorbate to the BNNTs can be explored. In particular, the surface reactivity at the PS and near a SW defect on BNNTs can be compared based on DFT calculations of chemical bonding. If the adsorbates are weakly physisorbed on the BNNTs, then the DFT/GGA method tends to underestimate the adsorption energy.[14,35,57,58] Therefore, in the case of physisorption, the basis-set superposition error (BSSE) corrections are not considered because of an already underestimated adsorption energy. Here, the results of adsorption energies are only semiquantitative for analyzing the trend of physisorption.

The adsorption or binding energy is defined as $BE = E_{tot}$(adsorbate + BNNT) − E_{tot}(adsorbate) − E_{tot}(BNNT), where E_{tot} denotes the total energy of the combined adsorbate/BNNT system. Thus, a negative (positive) *BE* denotes exothermic (endothermic) adsorption. The *BE* values and other properties are calculated only based on the lowest-energy structural configuration for the combined adsorbate/BNNT systems.

3. Results and Discussion

3.1. Geometrical Structures and Electronic Properties of Zigzag (8,0) and Armchair (5,5) BNNTs. Figure 1 shows the optimized structures of a pristine 16-layer zigzag (8,0) and a 13-layer armchair (5,5) BNNT model, with and without containing the SW defect. The buckling pattern of B−N sp^2 bonds in which N atoms slightly protrude B atoms to form a sawtooth-like sidewall surface is visible for the zigzag (8,0)-PS BNNT but not for the armchair (5,5)-PS BNNT, consistent with previous findings.[3] The SW defect is generated by rotating a B−N bond by 90° with four associated hexagons fused into two pentagon/heptagon pairs (5-7-7-5). Note that there are two possible SW defects, namely, straight SW [SW1, Figure 1a and b] and slanted SW [SW2, Figure 1c and d] defect, depending on the orientation of the rotated B−N bond.

The SW defect can cost larger formation energy than isolated pentagons or heptagons, which are more visible in CNTs and BNNTs.[51,59] As expected, our calculations show that defect-free BNNTs are the ground state for either zigzag or armchair BNNTs with the energy ranking PS(0.00 eV) < SW1(4.69 eV) < SW2(5.18 eV) and PS(0.00 eV) < SW2(4.94 eV) < SW1-(5.48 eV), respectively, showing that the SW defect gives rise to steric strain and frustrated B−B and N−N bonds. On the basis of the energy ranking, we chose (8,0)-SW1 and (5,5)-SW2 BNNTs as defect-containing models for adsorption study. The calculated bond lengths of adsorbates and those near the adsorption sites are collected in Table 1. It has been shown that the sidewall reactivity of CNTs toward the addition reaction increases linearly with pyramidalization angles,[27e] an indicator of deviation from sp^2 to sp^3 hybridization. Thus, the frustrated bonds combined with local strain and increased pyramidalization angles are expected to be more-reactive than normal B−N bonds.

The structural instability induced by a transformation from a normal B−N bond to frustrated B−B and N−N bonds is known as the bond frustration effect.[1,3] The bond-length measurements also show that the bond frustration effect is caused mainly by the local strain because a change in bond lengths occurs only for B−N bonds near the SW defect. The frustration energies associated with B−B and N−N bonds in BNNTs are much-higher than that (1.8 eV per frustrated bond) in a planar BN graphite-like sheet.[2a] Hence, the SW defects in BNNTs are less likely to form than in planar BN sheet.

To gain more insight into the effect of SW defects on the electronic properties of BNNTs, we plotted the density of states (DOS) for the two BNNT models. As shown in Figure 2, one SW defect on a 16-layer zigzag (8,0) and a 13-layer armchair (5,5) BNNT only moderately modifies the DOS of BNNTs compared to the DOS of pristine BNNTs. The HOMO−LUMO energy gaps for the zigzag (8,0) BNNTs decrease as PS(5.64 eV) > SW1(5.35 eV) > SW2(5.28 eV), whereas those for the armchair (5,5) BNNTs decrease as PS(6.80 eV) > SW2(5.71 eV) > SW1(5.46 eV). The calculated energy gaps from the cluster models are larger than those obtained from using PBCs,[4,37,40a,41d] suggesting that the defective BNNTs are still wide band-gap semiconductors. Recent UV−vis absorption experiments[41d] show that multiwalled BNNTs have an optical band-gap transition at 5.80 eV. Considering that realistic BNNTs likely contain defects, our calculated energy gaps are quite consistent with the experimental measurements.[41e] Figure 2a shows that the SW defect in the zigzag (8,0) BNNT brings little change in the DOS except a slightly decreased band gap, whereas that in the armchair (5,5) BNNT, the SW defect generates an impurity state (see arrows in Figure 2b) near the conduction-band (CB) edge.

3.2. Sidewall Reactivity at PS and near SW Defect. Tables 2−4 summarize calculated binding energy (*BE*), net charge transfer (δq), and the binding distance (*BD*) for the lowest-energy configuration of combined adsorbates/BNNTs. The corresponding local structures of the adsorbates are displayed in Figures 3, 4, 5, and 7, respectively. On the basis of the *BE* magnitude, we classify the physical nature of adsorption on the sidewall of BNNTs as atomic chemisorption, molecular chemisorption, and physisorption.

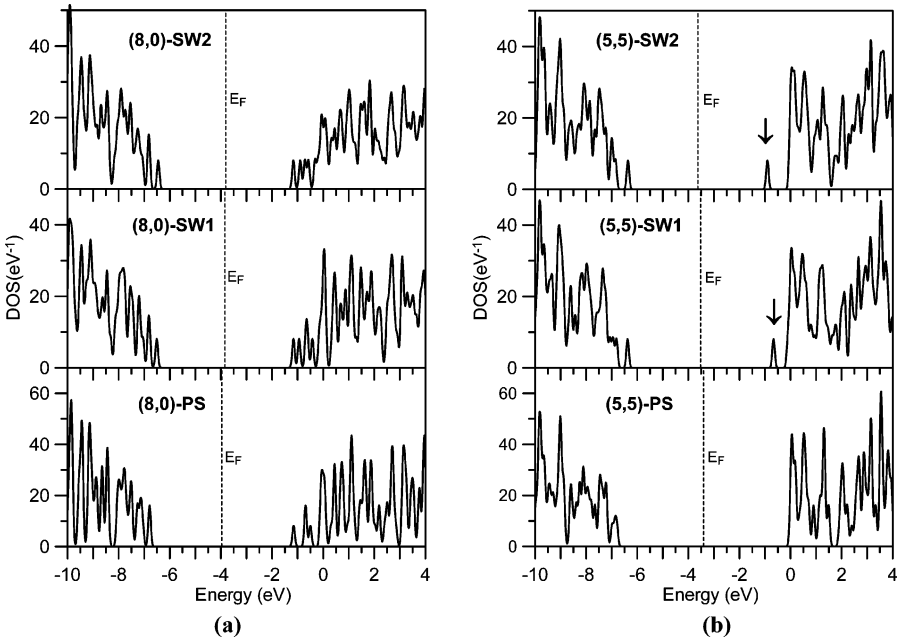

Figure 2. Density of states (DOS) for pristine single-walled zigzag (8,0) and armchair (5,5) BNNT models. E_F denotes Fermi levels, which are located at −3.97, −3.84, −3.81, −3.40, −3.52, and −3.63 eV for (8,0)-PS, (8,0)-SW1, (8,0)-SW2, (5,5)-PS, (5,5)-SW1, and (5,5)-SW2 BNNTs, respectively.

TABLE 2: Binding Energy (*BE*, in eV) for Various Adsorbates at PS and SW1 in Zigzag (8,0) BNNTs and at PS and SW2 in Armchair (5,5) BNNTs

	BE		*BE*	
adsorbate	(8,0)-PS	(8,0)-SW1	(5,5)-PS	(5,5)-SW2
H	−0.016	−1.12	0.00	−1.13
O	−2.36	−7.22	−2.63	−6.69
O_2	1.60	−2.38	1.39	−1.76
H_2O	−0.23	−0.24	−0.186	−0.24
NH_3	−0.68	−0.84	−0.55	−0.81
CO	−0.065	−0.102	−0.047	−0.102
H_2	−0.010	−0.017	−0.001	0.001

TABLE 3: Net Charge Transfer (δq) for Various Adsorbates at PS and SW1 in Zigzag (8,0) BNNTs and at PS and SW2 in Armchair (5,5) BNNTs

	δq(*e*)		δq(*e*)	
adsorbate	(8,0)-PS	(8,0)-SW1	(5,5)-PS	(5,5)-SW2
H	0.10	0.05	0.09	0.06
O	−0.41	−0.45	−0.41	−0.42
O_2	−0.56	−0.59	−0.52	−0.61
H_2O	0.06	0.15	0.05	0.14
NH_3	0.23	0.25	0.23	0.24
CO	0.02	0.12	0.02	0.12
H_2	0.00	0.008	0.00	0.00

TABLE 4: Binding Distance (*BD*, in Å) for Various Adsorbates at PS and SW1 in Zigzag (8,0) BNNTs and at PS and SW2 in Armchair (5,5) BNNTs

	BD		*BD*	
adsorbate	(8,0)-PS	(8,0)-SW1	(5,5)-PS	(5,5)-SW2
H	1.364	1.373	1.372	1.368
O	1.401	1.374	1.443	1.362
O_2	1.447	1.391	1.380	1.416
H_2O	2.509	1.859	2.649	1.941
NH_3	1.693	1.668	1.708	1.670
CO	3.129	1.601	3.171	1.598
H_2	3.536	3.212	3.304	3.153

3.2.1. Atomic Chemisorption of H and O Atoms and O_2. The atomic H and O are chemically much-more reactive than their molecular counterparts. However, it is still of fundamental interest to study the binding of atomic H and O to the BNNT sidewall because of their relevance to H_2, O_2, and H_2O adsorption and potential applications in hydrogen storage and chemical functionalizations.

Previous studies have shown that H can only bind to zigzag BNNTs with a *BE* of 0.32∼0.35 eV and a B−H bond length of 1.264 Å.[37,40a] However, our DFT calculations suggest nearly nonbinding of atomic H to the sidewall of defect-free BNNT, with *BE* values of −0.016 and 0.00 eV and B−H bond lengths of 1.364 and 1.372 Å for (8,0)-PS and (5,5)-PS BNNTs, respectively. For BNNTs containing defects, however, the binding of atomic H to the SW defects are strongly exothermic with *BE* values of −1.12 and −1.13 eV for (8,0)-SW1 and (5,5)-SW2 BNNTs, respectively. The B−H bond lengths are longer than those at the tube end (Table 1) and that of BH_3 [1.195 Å, calculated at PBE1PBE/6-31G(d, p) level], suggesting the formation of sp^3-hybridized B−H bond type. Note that the initial separation of the H atom from the BNNT sidewall was set at ∼1 Å in our calculations.

Atomic O species are highly reactive, compared to the ground-state (triplet) or excited (singlet) O_2 molecules. Indeed, atomic O can react with BNNTs easily to form B−O−N bond at a PS or B−O−B bond near a SW defect (Table 2 and Figure 3). The surface reactions at the PS are moderately exothermic with *BE* values of −2.36 and −2.63 eV for (8,0) and (5,5) BNNTs, respectively, whereas those near a SW defect are strongly exothermic with *BE* values of −7.22 and −6.69 eV for (8,0) and (5,5) BNNTs, respectively. These surface reactions are accompanied by 0.41−0.45*e* of charge transfer δq from BNNT to O because of the strong electronegativity of the O atom (see Table 3). Our calculations show that the frustrated B−B bonds are more susceptible to oxidation than normal B−N bonds. The favorable adsorption sites are located on top of the B1−B3 bonds near the SW defect and on top of the B−N bonds, which have the largest deviating angle from tube axis; that is, the B−N bond is perpendicular to tube axis in the armchair BNNT and slanted in the zigzag BNNT. These bonds are subjected to more strain and are active sites. The separations

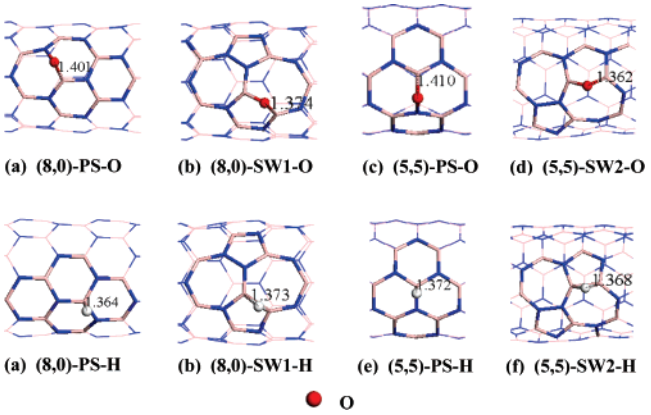

Figure 3. Lowest-energy configurations for atomic chemisorption of O and H on (8,0) and (5,5) BNNTs. The local structures of the adsorbate are displayed with binding distance (in Å) labeled.

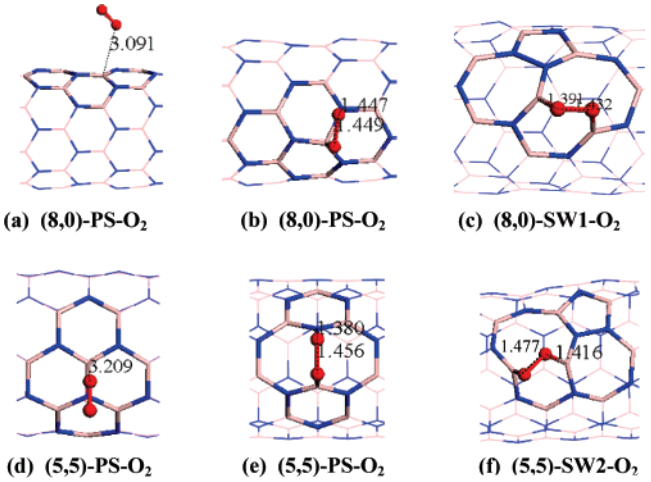

Figure 4. Lowest-energy configurations for molecular chemsorption of O_2 on (8,0) and (5, 5) BNNTs, as in Figure 3.

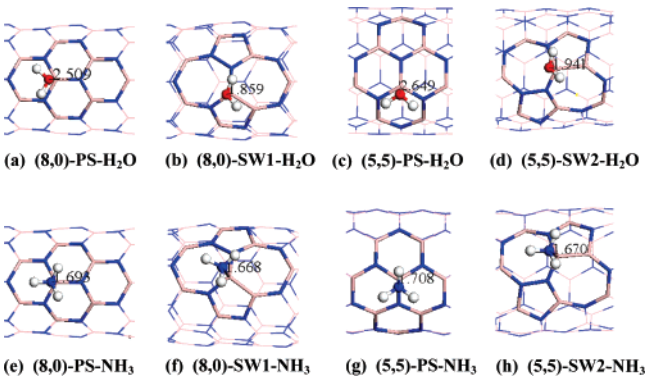

Figure 5. Lowest-energy configurations for molecular chemisorption of NH_3 and H_2O on (8,0) and (5, 5) BNNTs, as in Figure 3.

between the two B atoms (B1···B3) at the SW1 and SW2 defects, when bonded with the O atom, increase to 2.215 and 2.216 Å from their equilibrium bond lengths of 1.709 and 1.694 Å, respectively (Table 4).

Next, we studied adsorption of O_2 at a PS and near a SW defect on the sidewall of BNNTs. Figure 4 shows the adsorption configurations of O_2 on the sidewall of BNNTs. It is interesting to note that the PS and SW defects show distinct reactivity toward O_2 adsorption. At the PS, chemisorption of O_2 may occur under drastic reaction conditions because the chemisorption is endothermic with *BE* values of 1.60 and 1.39 eV for (8,0) and (5,5) BNNTs, respectively. Alternatively, physisorption of O_2 is more likely to occur at the PS because the adsorption is slightly exothermic [$BE = -0.039$ eV for (8,0) and $BE = -0.035$ eV for (5,5) BNNT]. In contrast, chemisorption of O_2 near SW defects on (8,0) and (5,5) BNNTs is energetically favorable with exothermic *BE* values of −2.38 and −1.76 eV, respectively. As in the case of atomic O adsorption, chemisorption of O_2 is also accompanied by notable δq from BNNT to O_2 (0.52−0.61*e*) (Table 3). Apparently, O_2 molecules act as a strong electron acceptors or as *p*-type impurities in wide-band-gap semiconductor BNNTs.

The binding characteristics of O_2 near SW1 and SW2 defects can be characterized as cycloaddition of O_2 where the two B−O bonds are formed with enhanced O−O bond lengths (1.432 and 1.477 Å, respectively) and enhanced B1···B3 bond separations (2.519 and 2.394 Å, respectively), leading to a distorted square-like B_2O_2 ring structure. Interestingly, such a distortion can make the LUMO lobes of singlet O_2 better match with the pronounced HOMO lobes localized at the B1−B3 bond with the same orbital symmetry (see arrows in Figure 6b and d). In contrast, the HOMO lobes of the ground-state (triplet) O_2 impose forbidden symmetry on the LUMO lobes of BNNTs, which might imply that the singlet state of O_2 is achieved by activation of the B1−B3 bridge bond prior to the reaction. This argument may be also applicable to the cycloaddition of O_2 at the PS, where the HOMO lobes (Figure 6a and c) are localized mainly near the N atoms (with larger electronegativities than the B atoms), leading to insufficient and energy-cost overlaps of the frontier orbitals of reactants. The endothermic process for the O_2 chemisorption at the PS is thus expected. Note that a previous experimental study[6] reported that BNNTs bear oxidation inertness. Further studies on the reaction pathway and oxidation near other types of defects such as B and N vacancies or doping sites[9] are needed to fully address this issue.

3.2.2. Molecular Chemisorption of H_2O and NH_3. Both H_2O and NH_3 are polar molecules with permanent dipole moments of 1.85 and 1.5 D, respectively. The two heteronuclear molecules can moderately bind to the sidewall of BNNTs at a PS and SW defect (Figure 5). The binding interactions can be described as molecular chemisorption because of their moderate exothermic *BE* values (Table 2), smaller δq from adsorbates to BNNTs (Table 3), some changes in B−N bond lengths at the adsorption site, and a shorter *BD* compared to typical physisorption (Table 4). As expected, the binding of H_2O and NH_3 to the sidewall of BNNTs are stronger near SW defects than at the PS.

For H_2O, the BE values are comparable (ca. −0.2 eV) at the PS and SW defect, suggesting that H_2O can be easily adsorbed onto or desorbed from the outer surface of BNNTs under ambient conditions. The charge transfer from H_2O to BNNT ($\delta q \sim 0.1e$) is small, consistent with soft Lewis-base nature of H_2O. It should be pointed out that the adsorption of single H_2O does not include the hydrogen-bond effect for which each hydrogen bond has an average energy of ∼0.22 eV.

NH_3 is known to be a strong Lewis base. The binding of NH_3 to the BNNTs is stronger than that of H_2O. On (8,0) BNNTs, the binding of NH_3 at the PS gives rise to a *BE* of −0.68 eV with a *BD* of 1.693 Å, indicating slightly stronger binding than that predicted previously using PBCs.[60] The binding of NH_3 to the SW1 defect is slightly stronger (−0.84 eV and 1.668 Å) than that at the PS. On (5,5) BNNTs, the binding of NH_3 follows the same trend as that on (8,0) BNNTs, that is, smaller *BE* (−0.55 eV) at the PS and larger *BE* (−0.81 eV) at SW2 defect. As an electron donor, NH_3 transfers a partial charge (0.23−0.25 *e*) to the electron-deficient B1 atom of the B1−N2 bonds at both PS and SW defects (Table 3 and Figure 5).

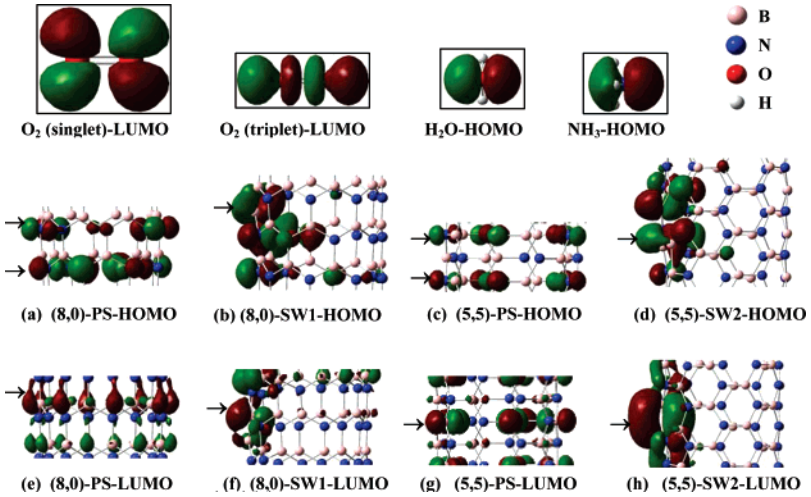

Figure 6. Calculated isosurfaces (isovalue = 0.03e/Å^3) of HOMOs (a−d) and LUMOs (e−h) for pristine zigzag (8,0) and armchair (5,5) BNNTs. Top panels are calculated isosurfaces (isovalue = 0.06e/Å^3) of LUMOs of O_2 (singlet and triplet) and HOMOs of H_2O and NH_3. Arrows are discussed in the text.

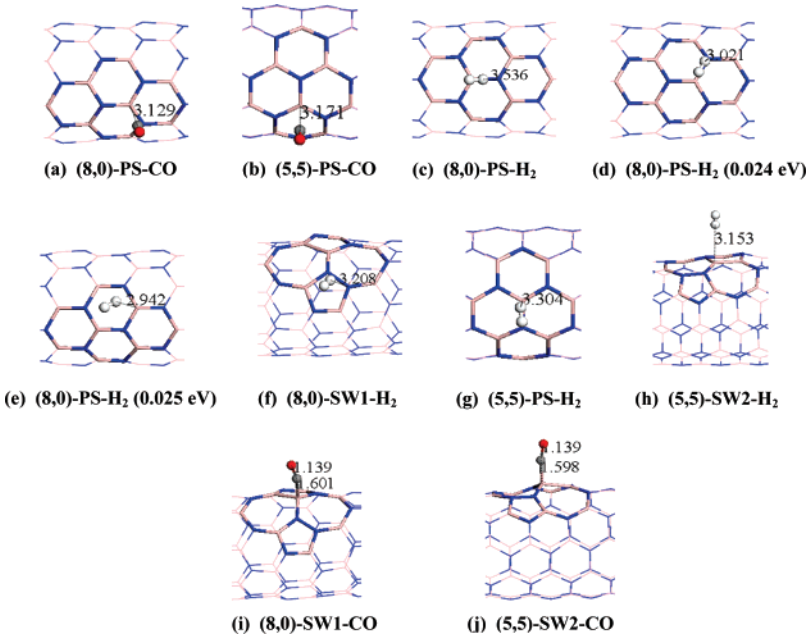

Figure 7. Lowest-energy configurations for physisorption of H_2 and CO on zigzag (8,0) and armchair (5,5) BNNTs, as in Figure 3. (d e) Two examples of H_2/(8,0)-PS BNNTs with shorter binding distances but higher total energies (in brackets) compared to the lowest-energy configuration (c).

In general, molecular chemisorption of NH_3 on the BNNT sidewall is stronger than H_2O, as indicated by the larger *BE* and δq and smaller *BD* for the former and consistent with their electron donor capability. The nature of molecular chemisorption can be also seen in the slightly enhanced bond lengths near the adsorption sites. For instance, upon adsorption of NH_3, the B1−N2, B1−B3, and B1−N6 bond lengths in (8,0)-SW1 BNNT are enhanced to 1.509, 1.752, and 1.538 Å from 1.420, 1.709, and 1.461 Å, respectively (Table 1).

The binding configurations are also consistent with the calculated HOMOs of NH_3 and H_2O and LUMOs of BNNTs (Figure 6), where the LUMOs are localized mainly onto B atoms (arrows in Figure 6). Particularly, the exohedral lobes of LUMOs near the SW defect are larger than those at the PS and are confined to the frustrated B1−B4 bond bridge sites, giving pronounced exposure to the HOMOs of adsorbed NH_3 and H_2O. This explains why the B atoms are preferable adsorption sites, at which the B···N binding stems from moderate interaction between HOMOs of NH_3 or H_2O with LUMOs of BNNT with the same orbital signs. However, because of the large energy gaps, that is, 5.47, 5.46, 6.62, and 5.72 eV between the HOMO of NH_3 and the LUMOs of 8,0-PS, (8,0)-SW1, (5,5)-PS, and (5,5)-SW2 BNNTs, respectively, no obvious orbital overlaps are seen. This electronic feature is also consistent with the previous finding for zigzag (8,0) BNNTs (refs 37b and 60). Nevertheless, molecular chemisorption of a single NH_3 does affect the electronic structures of BNNTs; the Fermi level is lifted slightly by 0.20, 0.44, 0.16, and 0.51 eV for (8,0)-PS, (8,0)-SW1, (5,5)-PS, and (5,5)-SW2 BNNTs, respectively. Hence, the NH_3 adsorbate acts as an *n*-type impurity.

3.2.3. Physisorption of CO and H_2. The binding of CO and H_2 to the sidewall of defect-free BNNT is very weak with estimated *BE* values in the range of 0.00 to −0.07 eV, negligible δq (Table 2 and 3), and >3 Å of *BD* values (Table 4 and Figure 7). The adsorption of H_2 near SW defects is also very weak with the same order of *BE* values as those at the PS. The adsorption of CO near SW defects is slightly stronger as indicated by shorter *BD* values (1.6 Å), larger *BE* values (−0.10

eV), and δq (0.12e). The adsorption of both CO and H_2 to the BNNT is essentially physical in nature, which stems from dispersion force and dipole-induced-dipole interaction. Our calculations also show that several physisorption configurations for CO (or H_2) are nearly isoenergetic, insensitive to the adsorption sites and adsorbate orientations. In Figure 7, only the most-stable configurations are displayed. Additionally, two other H_2/(8,0)-PS BNNT configurations with shorter *BD* values but higher total energies are included in d and e. Note that the initial separation distance of CO and H_2 from the BNNT sidewall is set at ~1.2 Å in our calculations. Considering that the DFT/GGA method tends to underestimate van der Waals interaction as pointed out in Section 2, our results of the *BE* values are merely to show that CO and H_2 cannot be chemisorbed on the sidewall of defect-free BNNTs.

4. Conclusions

We have performed DFT calculations to examine the adsorption and sidewall reactivity of zigzag (8,0) and armchair (5,5) BNNTs with various chemical species. As expected, SW defects are more reactive than PS because of the formation of frustrated bonds (B−B and N−N) and enhanced steric strain within the two pentagon/heptagon pairs. Both atomic H and O are chemically adsorbed on the sidewall of BNNTs except that atomic H is only weakly physisorbed at the PS. The ground-state O_2 molecules are preferentially adsorbed at the B−B bridge site of SW defects to form a distorted square-like ring B_2O_2 and may be also physisorbed at the PS. H_2O and NH_3 are molecularly chemisorbed on the sidewall of BNNTs, and the adsorption near the SW defects is stronger than that at the PS. As an electron donor, NH_3 adsorbate also acts as an *n*-type impurity. The difference in surface reactivity near SW defects and at the PS on the sidewall of BNNTs can be understood through analyzing interactions between the frontier orbitals of adsorbates and BNNTs. It is found that the B−B bridge site activates O_2 from the ground state (triplet) to the singlet state, leading to significant overlaps between the HOMOs of defective BNNTs and the LUMO of O_2 with the same orbital symmetry. As such, oxidation near SW defects is more favorable than that at the PS.

Acknowledgment. This research was supported in part by grants from DOE (DE-FG02-04ER46164), the Nebraska Research Initiative, and NSFC (no. 20628304), and by the Research Computing Facility at University of Nebraska-Lincoln.

References and Notes

(1) *Synthesis and Properties of Boron Nitride, Material Science Forum*; Pouch, J. J., Alterovitz, A., Eds.; Trans. Tech. Publ.: Switzerland, 1990; Vols. 54−55

(2) (a) Charlier, J.-Ch.; Blase, X.; Vita, A. De; Car, R. *Appl. Phys. A* **1999**, *68*, 267. (b) Blase, X.; Vita, A. De; Charlier, J.-Ch.; Car, R. *Phys. Rev. Lett.* **1998**, *80*, 1666.

(3) (a) Srivastava, D.; Menon, M.; Cho, K. *Phys. Rev. B* **2001**, *63*, 195413. (b) Menon, M.; Srivastava, D. *Chem. Phys. Lett.* **1999**, *307*, 407.

(4) Blase, X.; Rubio, A.; Louie, S. G.; Cohen, M. L. *Eur. Phys. Lett.* **1994**, *28*, 335.

(5) Blase, X.; Rubio, A.; Louie, S. G.; Cohen, M. L. *Phys. Rev. B* **1995**, *51*, 6868.

(6) Chen, Y.; Zou, J.; Campbell, S. J.; Caer, G. Le. *Appl. Phys. Lett.* **2004**, *84*, 2430.

(7) Saito, R.; Fujita, M.; Dresselhaus, G.; Dresselhaus, M. S. *Appl. Phys. Lett.* **1992**, *60*, 2204.

(8) Chopra, N. G.; Luyken, R. J.; Cherrey, K.; Crespi, V. H.; Cohen, M. L.; Louie, S. G.; Zettl, A. *Science* **1995**, *269*, 966.

(9) (a) Ma, R. Z.; Golberg, D.; Bando, Y.; Sasaki, T. *Philos. Trans. R. Soc. London, Ser. A* **2004**, *362*, 2161. (b) Terrones, M.; Romo-Herrera, M.; Cruz-Silva, E.; Lopez-Urias, F.; Munoz-Sandoval, E.; Velazquez-Salazar, J. J.; Terrones, H.; Bando, Y.; Golberg, D. *Mater. Today* **2007**, *10*, 40.

(10) (a) Dillon, A. C.; Jones, K. M.; Bekkedahl, T. A.; Kiang, C. H.; Bethune, D. S.; Heben, M. J. *Nature* **1997**, *386*, 377. (b) Zandonella, C. *Nature* **2001**, *410*, 734.

(11) Chen, P.; Wu, X.; Lin, J.; Tan, K. L. *Science* **1999**, *285*, 91.

(12) Lee, J. W.; Kim, H. S.; Lee, J. Y.; Kang, J. K. *Appl. Phys. Lett.* **2006**, *88*, 143126.

(13) Bienfait, M.; Zeppenfeld, P.; Dupont-Pavlovsky, N.; Muris, M.; Johnson, M. R.; Wilson, T.; DePies, M.; Vilches, O. E. *Phys. Rev. B* **2004**, *70*, 035410.

(14) Zhao, J.; Buldum, A.; Han, J.; Lu, J. P. *Nanotechnology* **2002**, *13*, 195.

(15) Peng, S.; Cho, K. *Nanotechnology* **2000**, *11*, 57.

(16) (a) Liu, H. J.; Chan, C. T.; Liu, Z. Y.; Shi, J. *Phys. Rev. B* **2005**, *72*, 075437. (b) Chan, S. P.; Chen, G.; Gong, X. G.; Liu, Z. F. *Phys. Rev. Lett.* **2003**, *90*, 086403.

(17) Arab, M.; Picaud, F.; Devel, M.; Ramseyer, C.; Girardet, C. *Phys. Rev. B* **2004**, *69*, 165401.

(18) Fujiwara, A.; Ishii, K.; Suematsu, H.; Kataura, H.; Maniwa, Y.; Suzuki, S.; Achiba, Y. *Chem. Phys. Lett.* **2001**, *336*, 205.

(19) Jiang, J.; Sandler, S. I. *Phys. Rev. B* **2003**, *68*, 245412.

(20) Feng, X.; Irle, S.; Witek, H.; Morokuma, K.; Vidic, R.; Borguet, E. *J. Am. Chem. Soc.* **2005**, *127*, 10533.

(21) Kong, J.; Franklin, N. R.; Chou, C.; Chaplin, M. G.; Peng, S.; Cho, K.; Dai, H. *Science* **2000**, *287*, 622.

(22) Chang, H.; Lee, J.; Lee, S. M.; Lee, Y. H. *Appl. Phys. Lett.* **2001**, *79*, 3863.

(23) (a) Mark, D.; Ellison, M. J.; Crotty, D. K.; Spray, R. L.; Tate, K. E. *J. Phys. Chem. B* **2004**, *108*, 7938. (b) Lu, J.; Nagase, S.; Maeda, Y.; Wakahara, T.; Nakahodo, T.; Akasaka, T.; Yu, D.; Gao, Z.; Han, R.; Ye, H. *Chem. Phys. Lett.* **2005**, *405*, 90.

(24) Seo, K.; Park, K. A.; Kim, C.; Han, S.; Kim, B.; Lee, Y. H. *J. Am. Chem. Soc.* **2005**, *127*, 15724.

(25) Maiti, A.; Andzelm, J.; Tanpipat, N.; von Allmen, P. *Phys. Rev. Lett.* **2001**, *87*, 155502.

(26) Jiang, J.; Sandler, S. I.; Schenk, M.; Smit, B. *Phys. Rev. B* **2005**, *72*, 045447.

(27) (a) Lu, X.; Chen, Z.; Schleyer, P. R. *J. Am. Chem. Soc.* **2005**, *127*, 20. (b) Zhou, Z.; Zhao, J.; Chen, Z.; Schleyer, P. R. *J. Phys. Chem. B* **2006**, *110*, 25678. (c) Zhou, Z.; Zhao, J.; Chen, Z.; Gao, X.; Yan, T.; Wen, B.; Schleyer, P. R. *J. Phys. Chem. B* **2006**, *110*, 13363. (d) Chen, Z.; Nagase, S.; Hirsch, A.; Haddon, R.C.; Thiel, W.; Schleyer, P. R. *Angew. Chem., Int. Ed.* **2004**, *43*, 1552. (e) Chen, Z.; Thiel, W.; Hirsch, A. *ChemPhysChem* **2003**, *1*, 93.

(28) Chen, L.; Johnson, J. K. *Phys. Rev. Lett.* **2005**, *94*, 125701.

(29) (a) Talapatra, S.; Krungleviciute, V.; Migone, A. D. *Phys. Rev. Lett.* **2002**, *89*, 246106; Kleinhammes, A.; Mao, S.; Yang, X.; Tang, X.; Shimoda, H.; Lu, J.; Zhou, O.; Wu, Y. *Phys. Rev. B* **2003**, *68*, 075418. (b) Simonyan, V. V.; Johnson, J. K.; Kuznetsova, A.; Yates, Jr, J. T. *J. Chem. Phys.* **2001**, *114*, 4180.

(30) Rols, S.; Johnson, M. R.; Zeppenfeld, P.; Bienfait, M.; Vilches, O. E.; Schneble, J. *Phys. Rev. B* **2005**, *71*, 155411.

(31) Yim, W. L.; Gong, X. G.; Liu, Z. F. *J. Phys. Chem. B* **2003**, *107*, 9363.

(32) Byl, O.; Kondratyuk, P.; Forth, S. T.; FitzGerald, S. A.; Chen, L.; Johnson, J. K.; Yates, J. T., J. *J. Am. Chem. Soc.* **2003**, *125*, 5889.

(33) Ma, R.; Bando, Y.; Zhu, H.; Sato, T.; Xu, C.; Wu, D. *J. Am. Chem. Soc.* **2002**, *124*, 7672.

(34) Han, S. S.; Kang, J. K.; Lee, H. M.; van Duin, A. C. T.; Goddard, W. A., III *J. Chem. Phys.* **2005**, *123*, 114704.

(35) Jhi, S. H.; Kwon, Y. K. *Phys. Rev. B* **2004**, *69*, 245407.

(36) Tang, C.; Bando, Y.; Ding, X.; Qi, S.; Golberg, D. *J. Am. Chem. Soc.* **2002**, *124*, 14550.

(37) (a) Wu, X. J.; Yang, J. L.; Hou, J. G.; Zhu, Q. S. *Phys. Rev. B* **2004**, *69*, 153411. (b) Wu, X. J.; Yang, J. L.; Hou, J. G.; Zhu, Q. S. *J. Chem. Phys.* **2004**, *121*, 8481. (c) Wu, X. J.; Yang, J. L.; Hou, J. G.; Zhu, Q. S. *J. Chem. Phys.* **2006**, *124*, 054706. (d) Xiang, H. J.; Yang, J. L.; Hou, J. G.; Zhu, Q. S. *Appl. Phys. Lett.* **2005**, *87*, 243113.

(38) Chen, X.; Gao, X. P.; Zhang, H.; Zhou, Z.; Hu, W. K.; Pan, G. L.; Zhu, H. Y.; Yan, T. Y.; Song, D. Y. *J. Phys. Chem. B* **2005**, *109*, 11525.

(39) Han, S. S.; Lee, S. H.; Kang, J. K.; Lee, H. M. *Phys. Rev. B* **2005**, *72*, 113402.

(40) (a) Zhang, J.; Loh, K. P.; Yang, S. W.; Wu, P. *Appl. Phys. Lett.* **2005**, *87*, 243105. (b) Liu, H.; Zhou, G.; Yan, Q.; Wu, J.; Gu, B. L.; Duan, W. *Phys. Rev. B* **2007**, *75*, 125410.

(41) (a) Zhi, C. Y.; Bando, Y.; Tang, C. C.; Honda, S.; Sato, K.; Huwahara, H.; Golberg, D. *Angew. Chem., Int. Ed.* **2005,** *44*, 7932. (b) Zhi, C. Y.; Bando, Y.; Tang, C. C.; Xie, R. G.; Sekiguchi, T.; Golberg, D. *J. Am. Chem. Soc.* **2005**, *127*, 15996. (c) Zhi, C. Y.; Bando, Y.; Tang, C. C.; Golberg, D. *J. Am. Chem. Soc.* **2005**, *127*, 17144. (d) Zhi, C. Y.; Bando, Y.; Tang, C. C.; Golberg, D. *Phys. Rev. B* **2006**, *74*, 153413. (e) Zobelli,

A.; Ewels, C. P.; Gloter, A.; Seifert, G.; Stephan, O.; Csillag, S.; Colliex, C. *Nano Lett.* **2006**, *6*, 1955.

(42) Xie, S. Y.; Wang, W.; Shiral Fernando, K. A.; Wang, X.; Lin, Y.; Sun, Y. P. *Chem. Commun.* **2005**, 3670.

(43) (a) Loiseau, A.; Willaime, F.; Demoncy, N.; Hug, G.; Pascard, H. *Phys. Rev. Lett.* **1996**, *76*, 4737. (b) Terauchi, M.; Tanaka, M.; Suzuki, K.; Ogino, A.; Kimura, K. *Chem. Phys. Lett.* **2000**, *324*, 359.

(44) (a) Golberg, D.; Bando, Y. *Appl. Phys. Lett.* **2001**, *79*, 415. (b) Golberg, D.; Bando, Y.; Eremets, M.; Takemura, K.; Kurashima, K.; Tamiya, K.; Yusa, H. *Chem. Phys. Lett.* **1997**, *279*, 191.

(45) Lee, R. S.; Gavillet, J.; Lamy de la Chapelle, M.; Loiseau, A.; Cochon, J.-L.; Pigache, D.; Thibault, J.; Willaime, F. *Phys. Rev. B* **2001**, *64*, 121405.

(46) Demczyk, B. G.; Cummings, T.; Zettl, A.; Ritchie, R. O. *Appl. Phys. Lett.* **2001**, *78*, 2772.

(47) Stone, A. J.; Wales, D. J. *Chem. Phys. Lett.* **1986**, *128*, 501.

(48) Bettinger, H. F.; Dumitrica, T.; Scuseria, G. E.; Yakobson, B. I. *Phys. Rev. B* **2002**, *65*, 041406.

(49) Miyamoto, Y.; Rubio, A.; Berber, S.; Yoon, M.; Tomanek, D. *Phys. Rev. B* **2004**, *69*, 121413.

(50) Golberg, D.; Bando, Y.; Eremets, M.; Takemura, K.; Kurashima, K.; Yusa, H. *Appl. Phys. Lett.* **1996**, *69*, 2045.

(51) Saito, Y.; Maida, M. *J. Phys. Chem. A* **1999**, *103*, 1291.

(52) Yoon, M.; Han, S.; Kim, G.; Lee, S. B.; Berber, S.; Osawa, E.; Ihm, J.; Terrones, M.; Banhart, F.; Charlier, J.-C.; Grobert, N.; Terrones, H.; Ajayan, P. M.; Tomanek, D. *Phys. Rev. Lett.* **2004**, *92*, 075504.

(53) (a)Bettinger, H. F. *J. Phys. Chem. B* **2005**, *109*, 6922. (b) Andzelm, J.; Maiti, A. *Chem. Phys. Lett.* **2006**, *421*, 58.

(54) (a) Wang, C.; Zhou, G.; Liu, H.; Wu, J.; Qiu, Y.; Gu, B. L.; Duan, W. *J. Phys. Chem. B* **2006**, *110*, 10266. (b) Zhao, M,; Xia, Y.; Lewis, J. P.; Mei, L. *J. Phys. Chem. B* **2004**, *108*, 9599.

(55) Frisch, M. J.; Trucks, G. W.; Schlegel, H. B.; Scuseria, G. E.; Robb, M. A.; Cheeseman, J. R.; Montgomery, J. A., Jr.; Vreven, T.; Kudin, K. N.; Burant, J. C.; Millam, J. M.; Iyengar, S. S.; Tomasi, J.; Barone, V.; Mennucci, B.; Cossi, M.; Scalmani, G.; Rega, N.; Petersson, G. A.; Nakatsuji, H.; Hada, M.; Ehara, M.; Toyota, K.; Fukuda, R.; Hasegawa, J.; Ishida, M.; Nakajima, T.; Honda, Y.; Kitao, O.; Nakai, H.; Klene, M.; Li, X.; Knox, J. E.; Hratchian, H. P.; Cross, J. B.; Bakken, V.; Adamo, C.; Jaramillo, J.; Gomperts, R.; Stratmann, R. E.; Yazyev, O.; Austin, A. J.; Cammi, R.; Pomelli, C.; Ochterski, J. W.; Ayala, P. Y.; Morokuma, K.; Voth, G. A.; Salvador, P.; Dannenberg, J. J.; Zakrzewski, V. G.; Dapprich, S.; Daniels, A. D.; Strain, M. C.; Farkas, O.; Malick, D. K.; Rabuck, A. D.; Raghavachari, K.; Foresman, J. B.; Ortiz, J. V.; Cui, Q.; Baboul, A. G.; Clifford, S.; Cioslowski, J.; Stefanov, B. B.; Liu, G.; Liashenko, A.; Piskorz, P.; Komaromi, I.; Martin, R. L.; Fox, D. J.; Keith, T.; Al-Laham, M. A.; Peng, C. Y.; Nanayakkara, A.; Challacombe, M.; Gill, P. M. W.; Johnson, B.; Chen, W.; Wong, M. W.; Gonzalez, C.; Pople, J. A. *Gaussian 03*, revision C.02; Gaussian, Inc.: Wallingford, CT, 2004.

(56) Perdew, J. P.; Burke, K.; Ernzerhof, M. *Phys. Rev. Lett.* **1996**, *77*, 3865.

(57) *Molecular Interactions-From van der Waals to Strongly Bound Complexes*; Scheiner, S., Ed.; John Wiley & Sons: England, 1997.

(58) (a) Rydberg, H.; Dion, M.; Jacobson, N.; Schröder, E.; Hyldgaard, P., P.; Simak, S. I.; Langreth, D. C.; Lundqvist, B. I. *Phys. Rev. Lett.* **2003**, *91*, 126402. (b) Kohn, W.; Meir, Y.; Makarov, D. E. *Phys. Rev. Lett.* **1998**, *80*, 4153. (c) Andersson, Y.; Langreth, D. C.; Lundqvist, B. I. *Phys. Rev. Lett.* **1996**, *76*, 102. (d) Hult, E.; Andersson, Y.; Lundqvist, B. I.; Langreth, D. C. *Phys. Rev. Lett.* **1996**, *77*, 2029. (e) Lin, C. S.; Zhang, R. Q.; Niehaus, T. A.; Frauenheim, Th. *J. Phys. Chem. C* **2007**, *111*, 4069.

(59) Iijima, S.; Ichihashi, T.; Ando, Y. *Nature* **1992**, *356*, 776.

(60) Wu, X. J.; An, W.; Zeng, X. C. *J. Am. Chem. Soc.* **2006**, *128*, 12001.